

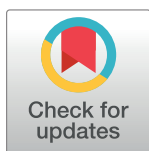
RESEARCH ARTICLE

Associations between regional blood-brain barrier permeability, aging, and Alzheimer's disease biomarkers in cognitively normal older adults

Marisa Denkinger^{1*}, Suzanne Baker², Ben Inglis³, Sarah Kobayashi¹, Alexis Juarez¹, Suzanne Mason¹, William Jagust^{1,2}

1 Helen Wills Neuroscience Institute, University of California, Berkeley, Berkeley, California, United States of America, **2** Lawrence Berkeley National Laboratory, Berkeley, California, United States of America, **3** Henry H. Wheeler Jr. Brain Imaging Center, University of California, Berkeley, Berkeley, California, United States of America

* marisa_becerra@berkeley.edu



OPEN ACCESS

Citation: Denkinger M, Baker S, Inglis B, Kobayashi S, Juarez A, Mason S, et al. (2024) Associations between regional blood-brain barrier permeability, aging, and Alzheimer's disease biomarkers in cognitively normal older adults. *PLoS ONE* 19(6): e0299764. <https://doi.org/10.1371/journal.pone.0299764>

Editor: Tamlyn Julie Watermeyer, University of Northumbria at Newcastle: Northumbria University, UNITED KINGDOM

Received: February 20, 2024

Accepted: May 5, 2024

Published: June 5, 2024

Copyright: © 2024 Denkinger et al. This is an open access article distributed under the terms of the [Creative Commons Attribution License](https://creativecommons.org/licenses/by/4.0/), which permits unrestricted use, distribution, and reproduction in any medium, provided the original author and source are credited.

Data Availability Statement: Our IRB requires a data use agreement for sharing of data. Because these data include MR images that could be used to identify individuals, we ask requestors to certify, among other considerations, that they will not attempt to re-identify individuals. For data requests, please contact Martin Boswell at msboswell@lbl.gov.

Abstract

Background

Increased blood-brain barrier permeability (BBBp) has been hypothesized as a feature of aging that may lead to the development of Alzheimer's disease (AD). We sought to identify the brain regions most vulnerable to greater BBBp during aging and examine their regional relationship with neuroimaging biomarkers of AD.

Methods

We studied 31 cognitively normal older adults (OA) and 10 young adults (YA) from the Berkeley Aging Cohort Study (BACS). Both OA and YA received dynamic contrast-enhanced MRI (DCE-MRI) to quantify K_{trans} values, as a measure of BBBp, in 37 brain regions across the cortex. The OA also received Pittsburgh compound B (PiB)-PET to create distribution volume ratios (DVR) images and flortaucipir (FTP)-PET to create partial volume corrected standardized uptake volume ratios (SUVR) images. Repeated measures ANOVA assessed the brain regions where OA showed greater BBBp than YA. In OA, K_{trans} values were compared based on sex, A β positivity status, and APOE4 carrier status within a composite region across the areas susceptible to aging. We used linear models and sparse canonical correlation analysis (SCCA) to examine the relationship between K_{trans} and AD biomarkers.

Results

OA showed greater BBBp than YA predominately in the temporal lobe, with some involvement of parietal, occipital and frontal lobes. Within an averaged ROI of affected regions, there was no difference in K_{trans} values based on sex or A β positivity, but OA who were APOE4 carriers had significantly higher K_{trans} values. There was no direct relationship

Funding: Research reported in this publication was supported by the National Institute On Aging of the National Institutes of Health under Award Number F31AG072872 and R01 AG080043. The funders had no role in study design, data collection and analysis, decision to publish, or preparation of the manuscript.

Competing interests: I have read the journal's policy and the authors of this manuscript have the following competing interests: Dr. Jagust has served as a consultant to Clario, Lilly and Eisai. Dr. Baker consults for Genentech. There are no other disclosures. This does not alter our adherence to PLOS ONE policies on sharing data and materials.

between averaged K_{trans} and global A β pathology, but there was a trend for an Ab status by tau interaction on K_{trans} in this region. SCCA showed increased K_{trans} was associated with increased PiB DVR, mainly in temporal and parietal brain regions. There was not a significant relationship between K_{trans} and FTP SUVR.

Discussion

Our findings indicate that the BBB shows regional vulnerability during normal aging that overlaps considerably with the pattern of AD pathology. Greater BBBp in brain regions affected in aging is related to APOE genotype and may also be related to the pathological accumulation of A β .

Introduction

Brain aging is accompanied by the aggregation of pathological proteins and the increasing prevalence of cerebrovascular disease. Recent research has shown that blood-brain barrier dysfunction is an important feature of both brain aging and Alzheimer's disease (AD). Blood-brain barrier permeability (BBBp) alteration in human aging and AD has been documented through the detection of blood-derived proteins in the hippocampus (HC) and cortex of AD patients and increases in the cerebrospinal fluid (CSF) of the plasma albumin protein ratio (Qalb) in both aging and AD [1–4]. More recent evidence of BBBp in humans comes from studies using the high spatial and temporal resolution imaging technique, dynamic contrast-enhanced magnetic resonance imaging (DCE-MRI), which allows measurement of subtle BBB changes [5]. A number of studies using DCE MRI have shown increased BBBp in both aging and AD with particular vulnerability of the hippocampus to this process [6–12]. Major questions remain, however, regarding the overall spatial distribution of BBBp, whether abnormalities are limited to the medial temporal lobe (MTL) and most importantly, whether or how BBBp is related to the development of AD.

Studies that explore the relationship between BBBp and AD benefit from the availability of fluid and PET biomarkers of the two protein aggregates associated with the disease – β -amyloid (A β) and pathological forms of tau. Higher BBBp measured with DCE-MRI in the HC and parahippocampal cortex (PHC) is evident before CSF measures of AD pathology, or cognitive decline [8]. Some evidence also suggests a lack of association between BBBp, measured using Qalb, and global A β PET in non demented older adults [1]. A recent study using DCE-MRI in cognitively normal and impaired individuals reported a lack of association of BBBp with A β or tau positivity, but a relationship with cognitive impairment and APOE4 genotype [13]. The discordance between in vivo measurement of BBBp and evidence of AD pathology suggests that increased BBBp may either be a very early precursor of AD, or lead to dementia symptoms through a mechanism independent of amyloid and tau pathology [14].

In this study, we investigated the relationship between BBBp and AD through 2 lines of evidence. First, we examined the full spatial distribution of BBBp which offers an ability to draw inferences about causal mechanisms and to help establish the role of BBBp in dementia. To do this, we compared BBB function in a group of cognitively normal older adults (OA) to young adults (YA) and mapped the whole brain distribution of BBBp. Second, we investigated whether BBBp in OA was associated with APOE4 genotype and regional A β and tau, measured using PET imaging.

Methods

Participants

We recruited 31 cognitively normal OA and 10 YA enrolled through the Berkeley Aging Cohort Study (BACS). OA participants were part of an ongoing longitudinal study of aging and received neuropsychological testing, DCE-MRI, and both A β and tau PET. We acquired PET scans an average of 2.4 months (SD = 5.3) before or after the DCE-MRI. YA participants received neuropsychological testing and DCE-MRI only. Inclusion criteria included a baseline Mini Mental State Examination (MMSE) score of >26, scores on all neuropsychological tests within 1.5 SD of age, sex and education adjusted norms, no neurological, psychiatric, or major medical illness, and no medications affecting cognitive ability.

Standard protocol approvals and participant consents

The project was approved by the institutional review board (IRB) at the University of California, Berkeley, and written informed consent was collected from each participant. The recruitment period for this study was 12/16/2019–6/23/2023.

MRI acquisition

1.5T MRI data were collected for standard PET processing at the Lawrence Berkeley National Laboratory (LBNL) on a Siemens Magnetom Avanto scanner. A whole-brain high resolution sagittal T1-weighted MPRAGE scan was acquired for each participant (TR = 2110 ms, TE = 3.58 ms, voxel size = 1mm isotropic, flip angle = 15°).

3T MRI data were collected at the UC Berkeley Henry H. Wheeler, Jr. Brain Imaging Center with a 3T Siemens Trio scanner and 32-channel head coil. We first collected high resolution sagittal T1-weighted magnetization prepared rapid gradient echo (MPRAGE) scans were acquired for each participant (repetition time (TR) = 2300 ms, inversion time (TI) = 900 ms, echo time (TE) = 2.96 ms, flip angle = 9°, voxel size = 1 mm isotropic, field of view (FOV) = 256 x 240 x 176 mm).

Next, baseline coronal T1-weighted maps, for DCE-MRI analysis, were acquired using a T1-weighted three-dimensional (3D) spoiled gradient echo pulse sequence and variable flip angle method (TR = 3.8 ms, TE = 1.64 ms, voxel size = 2.5 x 1.3 x 2.5 mm, FOV = 240 x 180 x 220 mm, flip angles = 2, 5, 10, 12, 15°) with full brain coverage. Coronal DCE-MRI were acquired with the same sequence and a flip angle of 5°. The sequence was repeated for a total of 21.3 minutes with a time resolution of 18 seconds [15]. The macrocyclic gadolinium-based contrast agent Gadobutrol (gadavist, 1 mmol/ml, 0.1ml/kg body weight) was administered intravenously over 30 seconds following the first 7 DCE repetitions.

PET acquisition

Methods for PET acquisition and analysis have been described previously, but are summarized here [16]. All PET scans were acquired at LBNL on a Siemens Biograph PET/CT scanner with the radiotracers [¹¹C]PiB for A β and [¹⁸F]Flortaucipir (FTP) for tau synthesized at LBNL's Biomedical Isotope Facility. Following acquisition of a CT scan, PiB-PET data were collected across 35 dynamic acquisition frames for 90 minutes after injection and FTP-PET data were binned into 4 x 5 minute frames from 80–100 minutes after injection. All PET images were reconstructed using an ordered subset expectation maximization algorithm, with attenuation correction, scatter correction, and smoothing with a 4 mm Gaussian kernel.

Structural MRI processing

The 3T T1-weighted images were segmented using FreeSurfer (FS) v7.1.1 (<http://surfer.nmr.mgh.harvard.edu/>) to derive anatomical ROIs in native space for the measurement of BBBp. Segmentations and parcellations were visually checked to ensure accuracy. FS Desikan-Killiany atlas ROIs were extracted and used to calculate region-specific BBBp. The 1.5T MRIs were used only for PET coregistration and were segmented in our standard processing pipeline to derive native space FS ROIs for PiB and FTP quantification.

DCE-MRI processing

All DCE-MRI processing was completed blind to all information except the participant's age and sex. DCE-MRI scans were realigned to the first image for motion correction using Statistical Parametric Mapping 12 (SPM12) prior to analysis. Analysis was completed using the DCE-MRI analysis software, ROCKETSHIP, running with Matlab [17]. The arterial input function (AIF) was manually labeled in each participant at the common carotid artery and was fitted with a bi-exponential function prior to kinetic modeling. A modified version of the Patlak linearized regression mathematical analysis was used to generate BBB permeability volume transfer constant (K_{trans}) maps [18]. This model provides high accuracy and precision for small permeability values [19, 20]. The total contrast agent concentration in the brain tissue, $C_{\text{tissue}}(t)$, can be described as a function of the contrast agent concentration in plasma, $C_{\text{AIF}}(t)$, the volume fraction of plasma, v_p , and the blood-to-brain volume transfer constant, K_{trans} , using the following equation:

$$C_{\text{tissue}}(t) = K_{\text{trans}} \int C_{\text{AIF}}(\tau) d\tau + v_p C_{\text{AIF}}(t)$$

K_{trans} thus represents the transport from the intravascular space to the extravascular extracellular space, with a higher K_{trans} indicating greater BBBp. K_{trans} was calculated at a voxelwise level for each subject and was averaged within FS Desikan-Killiany atlas ROIs.

PET processing

FTP images were realigned, averaged, and coregistered to the participant's 1.5T MRI using SPM12. Standardized uptake value ratio (SUVR) images were calculated by using the mean tracer uptake from 80–100 minutes post-injection and were normalized with an inferior cerebellar gray reference region [21]. The average SUVR values were calculated in FS Desikan-Killiany atlas ROIs derived from segmentation of the participant's MRI. This ROI data was partial volume corrected (PVC) using a modified Geometric Transfer Matrix approach and these values were used for analyses [21, 22].

PiB images were also realigned using SPM12. The frames from the first 20 minutes of acquisition were used for coregistration to the participant's 1.5T MRI. Distribution volume ratio (DVR) images for the PiB frames 35–90 minutes post injection were calculated using Logan Graphical analysis [23] and using whole cerebellar gray as a reference region. Global A β uptake was calculated using FS cortical ROIs [24]. A DVR of greater than 1.065 was used to classify participants as A β + [25]. We also calculated the mean DVR within a set of FS Desikan-Killiany atlas ROIs that reflect the typical pattern of A β deposition.

Statistical analyses

K_{trans} values were not normally distributed, as indicated by the Shapiro-Wilk's test; log transformation resulted in normally distributed data, which was used in subsequent analyses.

Statistical analyses were conducted using jamovi (<https://www.jamovi.org/>) and RStudio version 4.2.3 (<https://www.rstudio.com/>). To investigate regional differences in K_{trans} values between OA and YA, we ran a repeated measures analysis of variance (ANOVA) (group, region, and group X region), followed by post-hoc independent sample *t*-tests. [S1 Table](#) lists the 37 ROIs used in this analysis. We ran the analysis using K_{trans} values averaged across hemispheres, followed by right and left hemispheres comparisons in the OA. Subsequent analyses examining relationships between K_{trans} and AD biomarkers used only those regions where OA showed significantly larger K_{trans} values than YA. First, we created an averaged K_{trans} variable using these regions and reported comparisons between sex, $A\beta$ status, and *APOE4* carrier status. We also ran a linear model predicting averaged K_{trans} from EC FTP and an EC FTP by $A\beta$ status interaction, controlling for age and sex. We also ran the same model using FTP in a temporal meta-ROI [26].

Sparse Canonical Correlation Analysis (SCCA) was used to examine the multivariate regional relationships between BBBp and AD biomarkers, including PiB and FTP. SCCA is a variant of the traditional Canonical Correlation Analysis (CCA), which finds the optimal linear combinations of variables from two different modalities that are highly correlated with each other by weighting each variable to determine its significance in the correlation [27, 28]. The original variables are multiplied by these weights to form a multivariate projection. The canonical correlation is the correlation between these multivariate projections and multiple canonical correlations can be derived by using the residual data of the canonical variates to compute the subsequent canonical correlation. The first canonical correlation is usually the highest, capturing the maximum possible correlation between the two sets of variables. SCCA enhances CCA by incorporating sparsity constraints into the canonical vectors, often through penalties like the Lasso penalty. This process ensures that many weights in the canonical vectors are zero, highlighting the most significant variables in each modality contributing to the correlation.

We performed SCCA using the Penalized Multivariate Analysis (PMA) R package [29]. Bilateral K_{trans} , FTP, and PiB ROIs were chosen for analysis to reduce redundancy in the model. We used the 20 ROIs that were most affected by aging in our sample. The effects of age and sex were removed from the data by calculating the residuals, which were used for analyses. A lasso penalty of 0.5 was used to extract the most meaningful ROIs and we did not constrain any of the weights in the model to be positive or negative. The data were also mean centered and scaled. SCCA was performed separately for K_{trans} and PiB and K_{trans} and FTP. Significance was determined by correlating the multivariate projections of K_{trans} and AD biomarkers (PiB, FTP), which produces a correlation coefficient in each dimension. An F-approximation of Wilk's lambda was used as a test statistic and p-values < 0.05 were considered significant.

Data availability

Data will be made available to qualified investigators following publication of this study.

Results

Participant characteristics

The sample consisted of 31 OA (68–85 years old, mean 77.5, SD 5.2) and 10 YA (22–28 years old, mean 24.3, SD 2.3). [Table 1](#) shows the sample characteristics for OA and YA. Groups did not differ on years of education or sex. Within the OA group, 14 participants were classified as $A\beta+$, 4 as *APOE4* carriers, and 8 had treated hypertension (HTN). The range of partial volume corrected FTP values in the entorhinal cortex was 0.8–1.9 and in the temporal meta-ROI was 1.0–2.4.

Table 1. Participant demographics.

	Old (n = 31)	Young (n = 10)
Age, y**	77.5 ± 5.2	24.3 ± 2.3
Female	16 (52%)	3 (30%)
Years of education	17.6 ± 1.7	18.6 ± 2.1
MMSE*	28.4 ± 1.4	29.6 ± 0.9
APOE4 carriers	4 (14%); n = 28	n/a
Aβ+	14 (45%)	n/a
Global PiB (DVR)	1.1 ± 0.2	n/a
EC FTP (PVC SUVR)	1.4 ± 0.3	n/a
Temporal meta-ROI FTP (PVC SUVR)	1.4 ± 0.2	n/a

Abbreviations: MMSE = Mini-Mental State Examination; APOE4 = Apolipoprotein ε4; HTN = Hypertension. DVR = Distribution volume ratio; EC = Entorhinal cortex; PVC = Partial volume corrected; SUVR = Standardized uptake value ratio. Data shown as mean ± SD for continuous variables or n (%) for categorical variables. Group comparisons were run using independent sample *t*-tests or χ^2 tests.

* $p < 0.05$

** $p < 0.001$.

<https://doi.org/10.1371/journal.pone.0299764.t001>

Generation of K_{trans} maps

Fig 1 shows example whole brain K_{trans} maps in 2 OA and 2 YA participants with high and low BBBp (defined as the highest and lowest average K_{trans} from each group in averaged temporal, parietal, and occipital lobes). The 2 OA participants demonstrated larger K_{trans} values distributed throughout the cortex, compared to YA who had limited and more localized BBBp.

Differences in BBBp between OA and YA in cortical regions

A repeated measures ANOVA (age group, region, age group X region) across the BBBp average calculated in 37 bilateral FS-defined cortical ROIs showed a significant main effect of

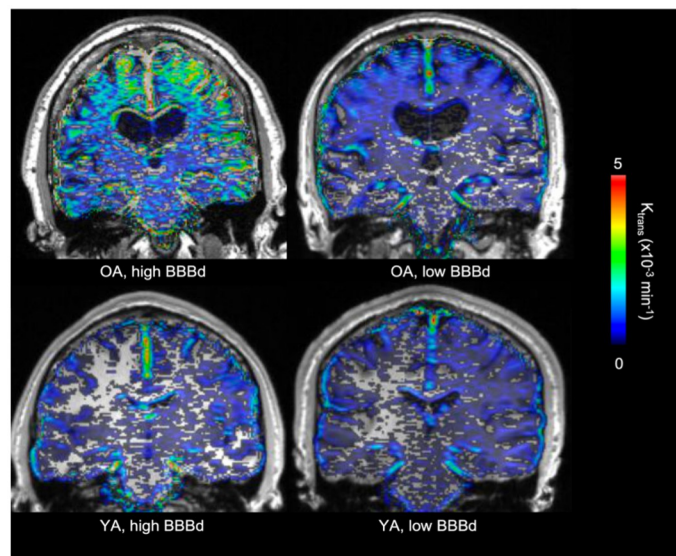


Fig 1. Voxelwise K_{trans} maps. Representative voxelwise BBB K_{trans} maps in 2 OA (top) and 2 YA (bottom) participants classified as having high and low BBBd. Color bar shows absolute K_{trans} values with units of min^{-1} .

<https://doi.org/10.1371/journal.pone.0299764.g001>

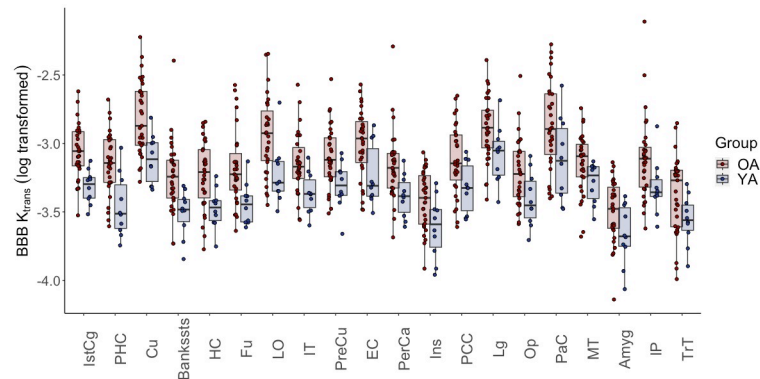


Fig 2. Regional BBBp in OA and YA. Repeated measures ANOVA revealed a significant age group by region interaction ($F = 2.1, p < 0.001$). The boxplot shows the regions where OA had significantly greater K_{trans} values following a post hoc independent sample t -test. Regions are ordered by largest to smallest effect size. Significance was defined as $p < 0.05$.

<https://doi.org/10.1371/journal.pone.0299764.g002>

region and an age group by region interaction ($F = 2.1, p < 0.001$). Post-hoc independent sample t -tests showed that OA had larger K_{trans} than YA in 20 regions bilaterally, that were largely in temporal and parietal cortex: (amygdala (Amyg), banks of the superior temporal sulcus (BanksSTS), entorhinal cortex (EC), fusiform gyrus (Fu), hippocampus (HC), insula (Ins), inferior temporal (IT), middle temporal (MT), parahippocampus (PHC), transverse temporal (TrT)), parietal (inferior parietal (IP), isthmus of the cingulate gyrus (IstCg), posterior cingulate (PCC), precuneus (PreCu)), and occipital lobes (cuneus (Cu), lateral occipital (LO), lingual (Lg), pericalcarine (PerCa)). There were also two regions in the frontal lobe where OA had larger K_{trans} (pars opercularis (Op), paracentral (PaC)) (Fig 2, all $p < 0.05$). Only the PHC and IstCg survived corrections for multiple comparisons ($p < 0.001$). We did not find any other regions with significant K_{trans} differences between groups, including white matter, nor were there any ROIs where YA had higher K_{trans} than OA. Effect sizes for the left and right hemisphere separately are shown in Fig 3. We used a paired samples t -test to compare left and right hemisphere K_{trans} values in the OA and found significantly larger K_{trans} in the left bankssts, Fu, HC, Ins, IP, IstCg, Lg, MT, PerCa, PHC, and TrT, with the bankssts, Fu, IstCg, IP, and PHC surviving corrections for multiple comparisons ($p < 0.001$). However, despite the hemispheric differences, the ranking order of regions by K_{trans} was relatively consistent between hemispheres. Therefore, we used averaged bilateral data for the rest of the analyses for a more streamlined analysis and to reduce the number of ROIs.

Averaged BBBp comparisons and correlations

Because of the significant age group \times region interaction and 20/37 ROIs showing significant differences between groups, we proceeded with an exploratory investigation of all ROIs showing differences, without multiple comparison correction. We created an averaged K_{trans} ROI consisting of the 20 regions where OA showed significantly larger K_{trans} than YA. Within the OA participants, there was no significant correlation between age and the averaged K_{trans} ROI ($R = 0.22, p = 0.34$). There were no significant averaged K_{trans} differences by sex ($t = -0.75, p = 0.46, d = -0.27$) or A β status ($t = -1.27, p = 0.21, d = -0.46$). There was also no significant relationship between averaged K_{trans} and global PiB index ($R = 0.32, p = 0.22$). We did find a significant difference by APOE4 status ($t = -2.50, p = 0.02, d = -1.53$, Fig 4), where APOE4 carriers had greater K_{trans} . There was no significant main effect of EC FTP or temporal meta-ROI

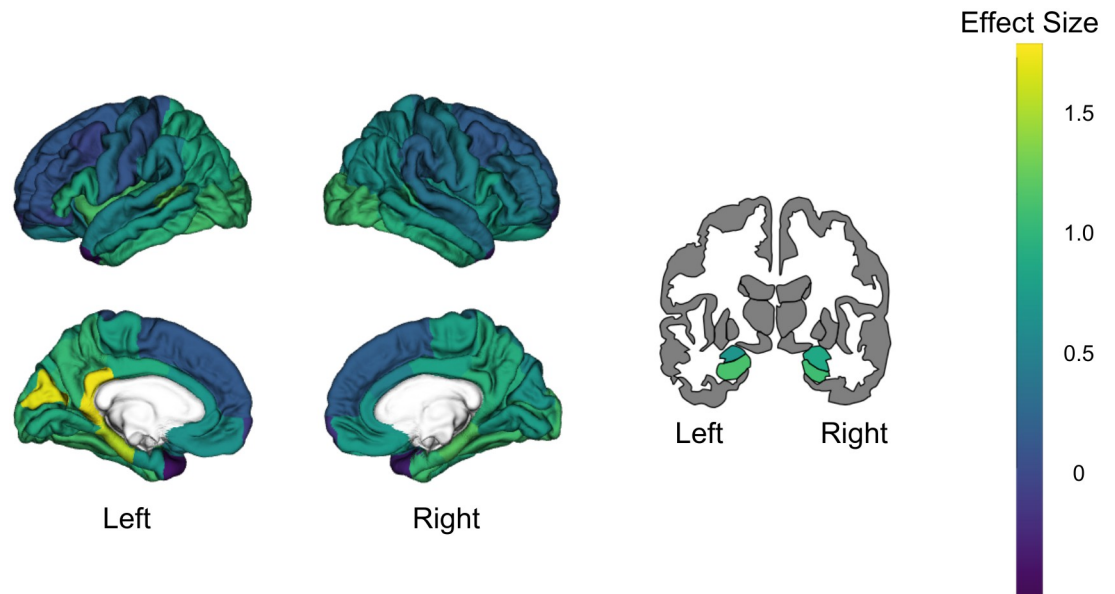


Fig 3. K_{trans} differences between OA and YA. Results from independent sample *t*-test comparing log transformed K_{trans} values in 74 FS ROIs between OA and YA. Brain plots show the Cohen's *d* effect size for each ROI. Effect sizes were overall larger in the left hemisphere than the right hemisphere.

<https://doi.org/10.1371/journal.pone.0299764.g003>

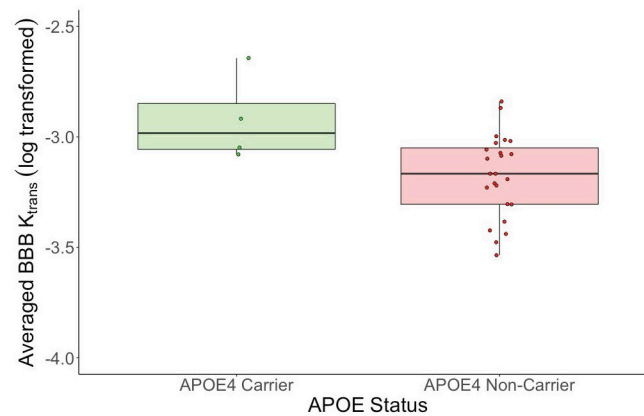


Fig 4. Effect of APOE status on averaged BBBp. Results from independent sample *t*-test comparing averaged K_{trans} and APOE4 carrier status. Averaged BBBp was significantly greater in the APOE4 carriers ($n = 4$) compared to non-carriers ($n = 24$) ($t = -2.50$, $p = 0.02$, $d = -1.53$).

<https://doi.org/10.1371/journal.pone.0299764.g004>

FTP on predicting averaged K_{trans} , but there was trend level interaction for EC FTP and A β status ($R = 0.41$, $p = 0.08$), as well as meta-ROI FTP and A β status ($R = 0.42$, $p = 0.08$).

Regional relationships between BBBd and AD biomarkers

Figs 5 and 6 show visual representations of the relationships between K_{trans} and AD biomarkers for the first three canonical correlation dimensions, and S2 and S3 Tables show the weights of each region that contributed to the dimension.

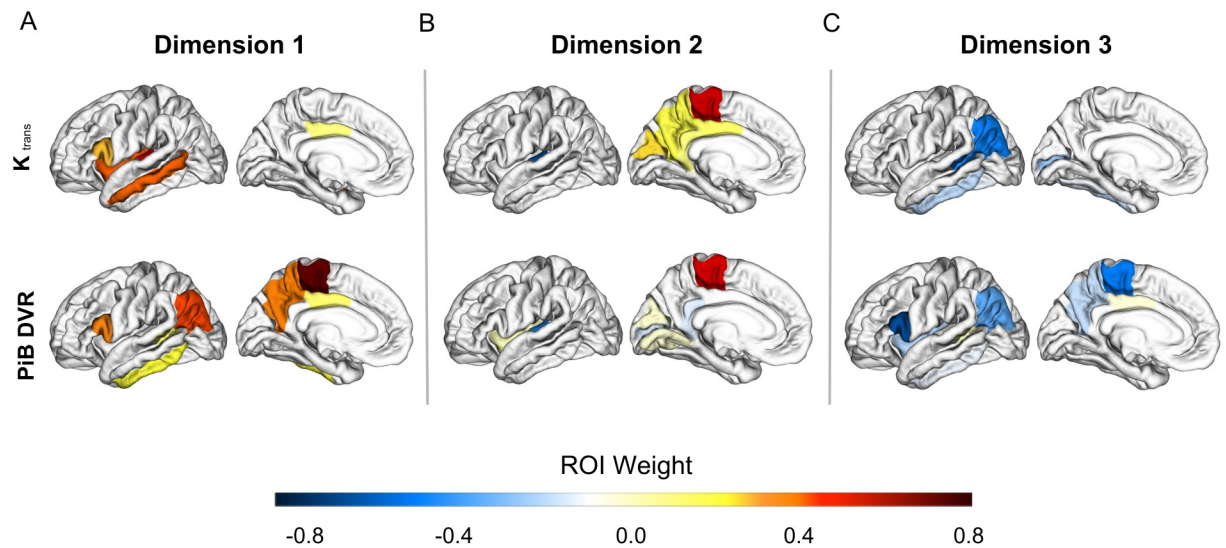


Fig 5. Associations between BBBp and A β . Brain plots show the first three dimensions from the sparse canonical correlation analysis between K_{trans} and PiB ROIs controlled for the effects of age and sex (A-C). (A) Dimension 1, $r = 0.39$, $F(9, 61) = 2.8$, $p = 0.009$ (B) Dimension 2, $r = 0.67$, $F(4, 52) = 5.2$, $p = 0.001$ (C) Dimension 3, $r = 0.26$, $F(1, 27) = 2.0$, $p = 0.17$. Dimensions represent K_{trans} changes (increase or decrease) aligned with corresponding PiB changes. Increases in a variable are signified by positive weights and decreases with negative weights. Regions are colored based on their weight and bilateral ROIs are depicted on a left hemisphere template brain. Weights reduced to zero due to sparsity constraints are not included in the color scale.

<https://doi.org/10.1371/journal.pone.0299764.g005>

The first two canonical correlations between K_{trans} and PiB were significant. Dimension 1 was represented by positive K_{trans} weights primarily in the temporal lobe and positive PiB weights mainly in temporal and parietal cortices (Fig 5A, $r = 0.39$, $F(9, 61) = 2.8$, $p = 0.009$), indicating a group of brain regions largely in temporal and parietal cortex where higher PiB

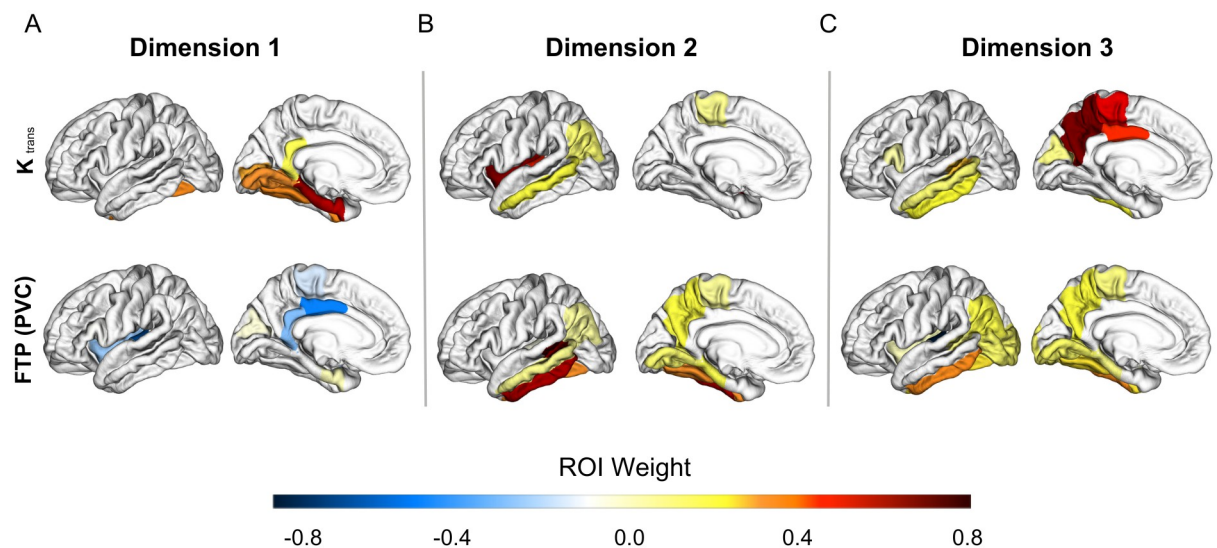


Fig 6. Associations between BBBp and tau. Brain plots show the first three dimensions from the sparse canonical correlation analysis between K_{trans} and partial volume corrected FTP ROIs controlled for the effects of age and sex (A-C). (A) Dimension 1, $r = 0.42$, $F(9, 61) = 1.5$, $p = 0.16$ (B) Dimension 2, $r = 0.30$, $F(4, 52) = 2.1$, $p = 0.09$ (C) Dimension 3, $r = 0.43$, $F(1, 27) = 6.3$, $p = 0.02$. Dimensions represent K_{trans} changes (increase or decrease) aligned with corresponding FTP changes. Increases in a variable are signified by positive weights and decreases with negative weights. Regions are colored based on their weight and bilateral ROIs are depicted on a left hemisphere template brain. Weights reduced to zero due to sparsity constraints are not included in the color scale.

<https://doi.org/10.1371/journal.pone.0299764.g006>

DVR was associated with higher K_{trans} in the temporal cortex and insula. Dimension 2 was represented by positive K_{trans} weights in the parietal cortex, but negative weights in the temporal cortex and mainly negative PiB weights in the temporal and occipital cortices (Fig 5B, $r = 0.67$, $F(4, 52) = 5.2$, $p = 0.001$). The dimension 3 correlation was not statistically significant (Fig 5C, $r = 0.26$, $F(1, 27) = 2.0$, $p = 0.17$).

Next, we looked at the associations between K_{trans} and partial volume corrected FTP in 20 regions. The correlation between K_{trans} and FTP in dimension 1 was not statistically significant (Fig 6A, $r = 0.42$, $F(9, 61) = 1.5$, $p = 0.16$). Dimension 2 showed a trend level correlation represented by positive K_{trans} weights mainly in the temporal lobe and positive FTP weights in the temporal and parietal cortices (Fig 6B, $r = 0.30$, $F(4, 52) = 2.1$, $p = 0.09$). Dimension 3 was represented by positive K_{trans} weights in lateral temporal and medial parietal regions and positive FTP weights in similar regions (Fig 6C, $r = 0.43$, $F(1, 27) = 6.3$, $p = 0.02$).

Discussion

Better characterization of BBBp during aging and its relationship, if any, to AD biomarkers is critical in understanding the role of neurovascular dysfunction in the AD pathological cascade. Using DCE-MRI in cognitively normal OA and YA, we showed that increased BBBp in aging does not occur globally, but rather occurred predominately in the temporal lobe, with involvement of the parietal, and less involvement of occipital and frontal lobes. In these regions we also found that APOE4 carriers had greater BBBp than non-carriers. PET imaging showed that BBBp has weak and inconsistent relationships with AD pathology. Although the large group of brain regions with elevated BBBp did not show any relationship to Ab, there was a trend for an A β by tau interaction on K_{trans} in this region, and the SCCA showed a pattern of regional relationships between K_{trans} and PiB DVR that recapitulated the known topography of AD pathology. Overall, these findings indicate that increased BBBp during aging occurs in overlapping regions affected in AD, is related to APOE genotype, and that it may be related to Ab pathology.

The regional BBBp we found strikingly reflects the pattern of brain vulnerability to AD pathology, particularly in regions that are affected early. Tau accumulation in normal aging begins in the medial temporal lobe and spreads to neighboring regions in the inferolateral temporal and medial parietal lobes in the presence of A β [16, 30]. The pattern of brain A β accumulation overlaps with the spatial location of tau best in later disease stages, covering regions in prefrontal, parietal, lateral temporal, and cingulate cortices. In line with previous studies [6–9, 12, 13], we saw greater BBBp in the MTL, particularly the EC, PHC, and HC, which accumulate tau pathology and undergo atrophy in normal aging, but do not typically accumulate A β at early stages of AD [31]. We also saw that in our sample the frontal lobe is relatively spared from increased BBBp, which is interesting because this brain region is associated with early A β accumulation [31], but late tau accumulation [32]. These differences suggest that increased BBBp follows a distribution pattern more like tau accumulation than Ab, with involvement of the MTL, temporal, parietal, and occipital lobes. The degree of BBBp alteration varied considerably in older individuals and increases were also seen in young adults, so it is difficult to say with certainty that these changes are pathological from these data alone. However, their associations with brain regions affected by AD and the suggestion of relationships with abnormal protein accumulation, raise concerns.

We next aimed to untangle the relationships between BBBp and neuroimaging measures of AD biomarkers. We found no significant difference in BBBp based on A β status in the pre-specified ROIs, although there was a significant APOE4 effect. We did not find any main effects of global A β , or regional tau in EC or temporal meta-ROI in predicting averaged K_{trans} .

However, we did find trend level interactions between A β status and tau, which suggests the possibility that the combined pathologies, which reflect the presence of AD, are related to BBBp. To further investigate the regional relationship between BBBp and AD biomarkers, we used a data driven SCCA approach. This method has the advantage of not requiring prespecified ROIs, and therefore may be able to detect subtle regional relationships. While this analysis did reveal some unique regional differences for the association between increased BBBp and increased A β , there was a distinct trend where most of the correlations occurred within the temporal and parietal cortices, regions known to be commonly affected by AD pathology. However, the spatial relationships between tau pathology and BBBp revealed through this statistical approach were weak. Altogether, we interpret our results as pointing towards complex relationships between Ab, tau and BBBp such that A β and BBBp could promote tau deposition over time, or A β and tau together could promote BBBp. Larger samples and longitudinal data will be necessary to establish these relationships.

The current evidence for a relationship between AD pathology and BBBp is conflicting. Existing studies use different methods for defining BBBp, and different ways of measuring AD pathology. Our findings of an effect of APOE4 genotype on BBBp replicate results of one study; this study did not find any consistent or trend level relationships between DCE-measured BBBp and A β or tau pathology measured with PET, but did find an APOE effect [13]. A previous study using MRI measures of water exchange to characterize BBBp showed an association between greater BBB permeability in frontal, parietal, and temporal regions, and evidence of A β accumulation, measured as reduced CSF A β 42 levels [33]. In a sample of patients with dementia, greater BBBp, measured using Q_{alb} , was associated with less CSF A β 42 and A β 40, but was not associated with CSF pTau181 or tTau [34]. However, another study using MRI measures of water exchange, found that greater BBBp was associated with increased CSF pTau [35]. These studies are difficult to compare to one another because of the methodological differences but suggest the possibility of relationships between AD pathology and alterations in BBB function.

Associations between BBBp and AD pathology have also been probed with animal models, which also can assess temporal relationships. Previous research found that BBB disruption leads to the deposition of A β by increasing its production and preventing its normal transport across the BBB [36, 37]. Studies in animal models have also shown that BBBp is increased before the presence of A β pathology in an AD mouse model [38] and that loss of pericytes increased brain A β 40 and A β 42 levels [39]. In contrast, another study found that excessive A β generation and deposition disrupts the BBB [40]. In the rTg4510 mouse model, BBB dysfunction emerged at the same time that perivascular tau emerged around major HC blood vessels and tau depletion eliminated BBBp [41]. Other research using human induced pluripotent stem cell-derived 3D organoids found that exposure to human serum, as a model of BBB disruption, increased tau phosphorylation [42]. Future longitudinal animal model studies examining relationships between these pathological proteins and BBBp have the potential for explaining relationships between these processes and revealing underlying mechanisms.

Although we used a technique for measuring BBBp that has high spatial and temporal resolution, along with state-of-the-art measures of AD pathology, our study does have limitations. The sample was small, especially in view of the number of brain regions investigated. Our statistical approach required multiple post-hoc tests, however this was justified by the significant group by region interaction. We also attempted to minimize this problem by using the multivariate method of sparse canonical correlation. Even though we investigated relationships between BBBp and AD biomarkers in many brain regions, the sparsity constraint ensured that only the most meaningful regions contributing to the canonical correlation were selected. The study of normal older participants, as opposed to those with AD, may also result

in smaller effect sizes, although this is offset by the importance of finding results in cognitively normal individuals. Importantly, even though we focused on cognitively normal older adults, the range of global PiB and FTP values in our sample has been enough to see biological effects in other studies [43, 44]. In this sample we only had 4 subjects who were APOE4 carriers, so future studies are needed to investigate the APOE effect further. Our sample also lacked diversity in terms of race/ethnicity and socioeconomic status, which limits the generalizability of these findings.

Taken together, our findings provide good evidence in support of previous work showing that aging is associated with increased BBBp. Furthermore, these alterations are not limited to MTL but include temporal and parietal cortical areas characteristically associated with AD pathology, especially tau. APOE4 appears to facilitate increased BBBp, but whether this occurs through a pathway related to AD pathology or independent of it is unclear. Consistent with previously reported data, relationships between AD pathology and BBBp are inconsistent and could reflect temporal lags between these processes, or an interaction between A β and tau pathology on BBBp that we cannot detect with our sample size. Nevertheless, these data point to important associations between aging, the spatial pattern of BBBp, and possible associations with AD pathology that require further investigation.

Supporting information

S1 Table. Regions of interest. Table listing the 37 FS Desikan-Killiany atlas ROIs used for analysis and their abbreviations.

(DOCX)

S2 Table. K_{trans} and PiB DVR weights for each region of interest in the SCCA.

ROI = region of interest. See [S1 Table](#) for a ROI abbreviation key.

(DOCX)

S3 Table. K_{trans} and FTP weights for each region of interest in the SCCA. PVC = partial volume corrected; ROI = region of interest. See [S1 Table](#) for a ROI abbreviation key.

(DOCX)

Author Contributions

Conceptualization: Marisa Denking, Suzanne Baker, Ben Inglis, William Jagust.

Data curation: Marisa Denking, Sarah Kobayashi, Alexis Juarez, Suzanne Mason, William Jagust.

Formal analysis: Marisa Denking, William Jagust.

Funding acquisition: Marisa Denking, William Jagust.

Investigation: Marisa Denking, Sarah Kobayashi, Alexis Juarez, Suzanne Mason, William Jagust.

Methodology: Marisa Denking, Suzanne Baker, Ben Inglis, William Jagust.

Writing – original draft: Marisa Denking, William Jagust.

Writing – review & editing: Marisa Denking, Suzanne Baker, Ben Inglis, Sarah Kobayashi, Alexis Juarez, Suzanne Mason, William Jagust.

References

1. Janelidze S, Hertze J, Nägga K, Nilsson K, Nilsson C, Wennström M, et al. (2017) Increased blood-brain barrier permeability is associated with dementia and diabetes but not amyloid pathology or APOE genotype. *Neurobiol Aging* 51:104–112 <https://doi.org/10.1016/j.neurobiolaging.2016.11.017> PMID: 28061383
2. Blennow K (1990) Blood-brain barrier disturbance in patients with Alzheimer's disease is related to vascular factors. *Acta Neurol Scand* 81:323–326 <https://doi.org/10.1111/j.1600-0404.1990.tb01563.x> PMID: 2360400
3. Erickson MA, Banks WA (2013) Blood—Brain Barrier Dysfunction as a Cause and Consequence of Alzheimer's Disease. *J Cereb Blood Flow Metab* 33:1500–1513 <https://doi.org/10.1038/jcbfm.2013.135> PMID: 23921899
4. Sengillo JD, Winkler EA, Walker CT, Sullivan JS, Johnson M, Zlokovic BV (2013) Deficiency in Mural Vascular Cells Coincides with Blood-Brain Barrier Disruption in Alzheimer's Disease: Pericytes in Alzheimer's Disease. *Brain Pathol* 23:303–310
5. Heye AK, Culling RD, del Valdés Hernández M C, Thrippleton MJ, Wardlaw JM (2014) Assessment of blood—brain barrier disruption using dynamic contrast-enhanced MRI. A systematic review. *Neuro-Image Clin* 6:262–274 <https://doi.org/10.1016/j.nicl.2014.09.002> PMID: 25379439
6. Montagne A, Barnes SR, Sweeney MD, et al. (2015) Blood-Brain Barrier Breakdown in the Aging Human Hippocampus. *Neuron* 85:296–302 <https://doi.org/10.1016/j.neuron.2014.12.032> PMID: 25611508
7. Moon W-J, Lim C, Ha IH, Kim Y, Moon Y, Kim H-J, Han S-H (2021) Hippocampal blood—brain barrier permeability is related to the APOE4 mutation status of elderly individuals without dementia. *J Cereb Blood Flow Metab* 41:1351–1361 <https://doi.org/10.1177/0271678X20952012> PMID: 32936729
8. Nation DA, Sweeney MD, Montagne A, et al. (2019) Blood—brain barrier breakdown is an early biomarker of human cognitive dysfunction. *Nat Med* 25:270–276 <https://doi.org/10.1038/s41591-018-0297-y> PMID: 30643288
9. Senatorov VVS, Friedman AR, Milikovsky DZ, et al (2019) Blood-brain barrier dysfunction in aging induces hyperactivation of TGF β signaling and chronic yet reversible neural dysfunction. *Sci Transl Med* 15
10. Starr JM, Farrall AJ, Armitage P, McGurn B, Wardlaw J (2009) Blood—brain barrier permeability in Alzheimer's disease: a case—control MRI study. *Psychiatry Res Neuroimaging* 171:232–241 <https://doi.org/10.1016/j.pscychresns.2008.04.003> PMID: 19211227
11. van de Haar HJ, Burgmans S, Jansen JFA, van Osch MJP, van Buchem MA, Muller M, et al. (2016) Blood-Brain Barrier Leakage in Patients with Early Alzheimer Disease. *Radiology* 281:527–535 <https://doi.org/10.1148/radiol.2016152244> PMID: 27243267
12. Verheggen ICM, de Jong JJA, van Boxtel MPJ, Gronenschild EHBM, Palm WM, Postma AA, et al. (2020) Increase in blood—brain barrier leakage in healthy, older adults. *GeroScience* 42:1183–1193
13. Montagne A, Nation DA, Sagare AP, et al (2020) APOE4 leads to blood—brain barrier dysfunction predicting cognitive decline. *Nature* 581:71–76 <https://doi.org/10.1038/s41586-020-2247-3> PMID: 32376954
14. Sweeney MD, Sagare AP, Zlokovic BV (2018) Blood—brain barrier breakdown in Alzheimer disease and other neurodegenerative disorders. *Nat Rev Neurol* 14:133–150 <https://doi.org/10.1038/nrneurol.2017.188> PMID: 29377008
15. Thrippleton MJ, Backes WH, Sourbron S, et al (2019) Quantifying blood-brain barrier leakage in small vessel disease: Review and consensus recommendations. *Alzheimers Dement* 15:840–858 <https://doi.org/10.1016/j.jalz.2019.01.013> PMID: 31031101
16. Schöll M, Lockhart SN, Schonhaut DR, et al (2016) PET Imaging of Tau Deposition in the Aging Human Brain. *Neuron* 89:971–982 <https://doi.org/10.1016/j.neuron.2016.01.028> PMID: 26938442
17. Barnes SR, Ng TSC, Santa-Maria N, Montagne A, Zlokovic BV, Jacobs RE (2015) ROCKETSHIP: a flexible and modular software tool for the planning, processing and analysis of dynamic MRI studies. *BMC Med Imaging* 15:19 <https://doi.org/10.1186/s12880-015-0062-3> PMID: 26076957
18. Patlak CS, Blasberg RG, Fenstermacher JD (1983) Graphical Evaluation of Blood-to-Brain Transfer Constants from Multiple-Time Uptake Data. *J Cereb Blood Flow Metab* 3:1–7 <https://doi.org/10.1038/jcbfm.1983.1> PMID: 6822610
19. Cramer SP, Larsson HB (2014) Accurate Determination of Blood—Brain Barrier Permeability Using Dynamic Contrast-Enhanced T1-Weighted MRI: A Simulation and *in vivo* Study on Healthy Subjects and Multiple Sclerosis Patients. *J Cereb Blood Flow Metab* 34:1655–1665

20. Heye AK, Thrippleton MJ, Armitage PA, del Valdés Hernández M C, Makin SD, Glatz A, et al. (2016) Tracer kinetic modelling for DCE-MRI quantification of subtle blood—brain barrier permeability. *NeuroImage* 125:446–455 <https://doi.org/10.1016/j.neuroimage.2015.10.018> PMID: 26477653
21. Baker SL, Maass A, Jagust WJ (2017) Considerations and code for partial volume correcting [¹⁸F]-AV-1451 tau PET data. *Data Brief* 15:648–657
22. Rousset OG, Ma Y, Evans AC (1997) Correction for Partial Volume Effects in PET: Principle and Validation. *J Nucl Med* 39:904–911
23. Logan J, Fowler JS, Volkow ND, Wang G-J, Ding Y-S, Alexoff DL (1996) Distribution Volume Ratios without Blood Sampling from Graphical Analysis of PET Data. *J Cereb Blood Flow Metab* 16:834–840 <https://doi.org/10.1097/00004647-199609000-00008> PMID: 8784228
24. Mormino EC, Brandel MG, Madison CM, Rabinovici GD, Marks S, Baker SL, et al. (2012) Not quite PIB-positive, not quite PIB-negative: Slight PIB elevations in elderly normal control subjects are biologically relevant. *NeuroImage* 59:1152–1160 <https://doi.org/10.1016/j.neuroimage.2011.07.098> PMID: 21884802
25. Villeneuve S, Rabinovici GD, Cohn-Sheehy BI, et al (2015) Existing Pittsburgh Compound-B positron emission tomography thresholds are too high: statistical and pathological evaluation. *Brain* 138:2020–2033 <https://doi.org/10.1093/brain/awv112> PMID: 25953778
26. Jack CR, Wiste HJ, Weigand SD, et al (2017) Defining imaging biomarker cut points for brain aging and Alzheimer's disease. *Alzheimers Dement* 13:205–216 <https://doi.org/10.1016/j.jalz.2016.08.005> PMID: 27697430
27. Härdle WK, Simar L (2015) *Applied Multivariate Statistical Analysis*. <https://doi.org/10.1007/978-3-662-45171-7>
28. Hotelling Harold (1936) Relations Between Two Sets of Variates. *Biometrika* 28:321–377
29. Witten DM, Tibshirani R, Hastie T (2009) A penalized matrix decomposition, with applications to sparse principal components and canonical correlation analysis. *Biostatistics* 10:515–534 <https://doi.org/10.1093/biostatistics/kxp008> PMID: 19377034
30. Sanchez JS, Becker JA, Jacobs HIL, et al (2021) The cortical origin and initial spread of medial temporal tauopathy in Alzheimer's disease assessed with positron emission tomography. *Sci Transl Med* 13: eabc0655 <https://doi.org/10.1126/scitranslmed.abc0655> PMID: 33472953
31. LaPoint MR, Baker SL, Landau SM, Harrison TM, Jagust WJ (2022) Rates of β -amyloid deposition indicate widespread simultaneous accumulation throughout the brain. *Neurobiol Aging* 115:1–11
32. Braak H, Braak E (1991) Neuropathological staging of Alzheimer-related changes. *Acta Neuropathol (Berl)* 82:239–259 <https://doi.org/10.1007/BF00308809> PMID: 1759558
33. Gold BT, Shao X, Sudduth TL, Jicha GA, Wilcock DM, Seago ER, et al. (2021) Water exchange rate across the blood-brain barrier is associated with CSF amyloid- β 42 in healthy older adults. *Alzheimers Dement* 17:2020–2029
34. Gan J, Yang X, Zhang G, Li X, Liu S, Zhang W, Ji Y (2023) Alzheimer's disease pathology: pathways between chronic vascular risk factors and blood-brain barrier dysfunction in a cohort of patients with different types of dementia. *Front Aging Neurosci* 15:1088140 <https://doi.org/10.3389/fnagi.2023.1088140> PMID: 37213537
35. Lin Z, Sur S, Liu P, et al (2021) Blood—Brain Barrier Breakdown in Relationship to Alzheimer and Vascular Disease. *Ann Neurol* 90:227–238 <https://doi.org/10.1002/ana.26134> PMID: 34041783
36. Ridler C (2018) BACE1 inhibitors block new A β plaque formation. *Nat Rev Neurol* 14:126–126
37. Wang H, Chen F, Du Y-F, Long Y, Reed MN, Hu M, et al. (2018) Targeted inhibition of RAGE reduces amyloid- β influx across the blood-brain barrier and improves cognitive deficits in db/db mice. *Neuropharmacology* 131:143–153
38. Ujiié M, Dickstein DL, Carlow DA, Jefferies WA (2003) Blood-Brain Barrier Permeability Precedes Senile Plaque Formation in an Alzheimer Disease Model. *Microcirculation* 10:463–470 <https://doi.org/10.1038/sj.mn.7800212> PMID: 14745459
39. Sagare AP, Bell RD, Zhao Z, Ma Q, Winkler EA, Ramanathan A, et al. (2013) Pericyte loss influences Alzheimer-like neurodegeneration in mice. *Nat Commun* 4:2932 <https://doi.org/10.1038/ncomms3932> PMID: 24336108
40. Montagne A, Zhao Z, Zlokovic BV (2017) Alzheimer's disease: A matter of blood—brain barrier dysfunction? *J Exp Med* 214:3151–3169 <https://doi.org/10.1084/jem.20171406> PMID: 29061693
41. Blair LJ, Frauen HD, Zhang B, et al (2015) Tau depletion prevents progressive blood-brain barrier damage in a mouse model of tauopathy. *Acta Neuropathol Commun* 3:8 <https://doi.org/10.1186/s40478-015-0186-2> PMID: 25775028

42. Chen X, Sun G, Tian E, Zhang M, Davtyan H, Beach TG, et al. (2021) Modeling Sporadic Alzheimer's Disease in Human Brain Organoids under Serum Exposure. *Adv Sci* 8:2101462 <https://doi.org/10.1002/adv.202101462> PMID: 34337898
43. Giorgio J, Adams JN, Maass A, Jagust WJ, Breakspear M (2023) Amyloid induced hyperexcitability in default mode network drives medial temporal hyperactivity and early tau accumulation. *Neuron* S0896627323008887 <https://doi.org/10.1016/j.neuron.2023.11.014> PMID: 38096815
44. Cassady KE, Chen X, Adams JN, Harrison TM, Zhuang K, Maass A, et al. (2023) Effect of Alzheimer's Pathology on Task-Related Brain Network Reconfiguration in Aging. *J Neurosci* 43:6553–6563 <https://doi.org/10.1523/JNEUROSCI.0023-23.2023> PMID: 37604690